

Insulin Receptor Substrate 2 (IRS2)-Deficient Mice Show Sensorineural Hearing Loss That Is Delayed by Concomitant Protein Tyrosine Phosphatase 1B (PTP1B) Loss of Function

Silvia Murillo-Cuesta,^{1,2,3} Guadalupe Camarero,^{1,2,3} Águeda González-Rodríguez,^{1,3,4} Lourdes Rodríguez-de la Rosa,^{1,2,3} Deborah J Burks,^{4,5} Carlos Avendaño,^{3,6} Ángela M Valverde,^{1,3,4} and Isabel Varela-Nieto^{1,2,3}

¹Institute of Biomedical Research “Alberto Sols” (IIBM), Spanish National Research Council–Autonomous University of Madrid (CSIC-UAM), Madrid, Spain; ²Centre for Biomedical Network Research on Rare Diseases (CIBERER), Institute of Health Carlos III (ISCIII), Valencia, Spain; Hospital La Paz Institute for Health Research (IdiPAZ), Madrid, Spain; ⁴Spanish Biomedical Research Centre in Diabetes and Associated Metabolic Disorders (CIBERDEM), ISCIII, Barcelona, Spain; ⁵Research Center Príncipe Felipe, Valencia, Spain; and the ⁶Department of Anatomy, Histology and Neuroscience, Medical School, Autonomous University of Madrid, Madrid, Spain

The insulin receptor substrate (IRS) proteins are key mediators of insulin and insulinlike growth factor 1 (IGF-1) signaling. Protein tyrosine phosphatase (PTP)-1B dephosphorylates and inactivates both insulin and IGF-1 receptors. IRS2-deficient mice present altered hepatic insulin signaling and β -cell failure and develop type 2-like diabetes. In addition, IRS2 deficiency leads to developmental defects in the nervous system. *IGF1* gene mutations cause syndromic sensorineural hearing loss in humans and mice. However, the involvement of IRS2 and PTP1B, two IGF-1 downstream signaling mediators, in hearing onset and loss has not been studied. Our objective was to study the hearing function and cochlear morphology of *Irs2*-null mice and the impact of PTP1B deficiency. We have studied the auditory brainstem responses and the cochlear morphology of systemic *Irs2*^{-/-}*Ptpn1*^{+/+}, *Irs2*^{+/+}*Ptpn1*^{-/-} and *Irs2*^{-/-}*Ptpn1*^{-/-} mice at different postnatal ages. The results indicated that *Irs2*^{-/-}*Ptpn1*^{+/+} mice present a profound congenital sensorineural deafness before the onset of diabetes and altered cochlear morphology with hypoinnervation of the cochlear ganglion and aberrant stria vascularis, compared with wild-type mice. Simultaneous PTP1B deficiency in *Irs2*^{-/-}*Ptpn1*^{-/-} mice delays the onset of deafness. We show for the first time that IRS2 is essential for hearing and that PTP1B inhibition may be useful for treating deafness associated with hyperglycemia and type 2 diabetes.

Online address: <http://www.molmed.org>

doi: 10.2119/molmed.2011.00328

INTRODUCTION

The insulin receptor substrate (IRS) proteins are key molecules in the signaling pathways induced by insulin and insulinlike growth factor 1 (IGF-1) and mediate their pleiotropic effects, including cell growth, survival, development and glucose metabolism (1).

Among the six known IRS proteins, IRS1 and IRS2 serve as adaptor proteins

to both the insulin receptor (IR) and the IGF-1 receptor (IGF1R), activating the phosphatidylinositol 3-kinase and mitogen-activated protein kinase (MAPK) pathways (2). Although IRS1 and IRS2 share similar expression patterns in most tissues, several lines of evidence suggest that IRS-mediated signaling in growth and metabolism is tissue specific (3,4). Mutations in IR and IGF1R lead to severe

defects in development and premature death in mice and humans (5,6). However, deletion of mouse IRS proteins 1 and 2 produces growth retardation and type 2 diabetes in mice, respectively (7,8).

IRS2 integrates the effects of insulin in peripheral target tissues, mainly the liver, with those of IGF-1 in pancreatic β cells to maintain glucose homeostasis. Mice lacking IRS2 exhibit impaired suppression of hepatic glucose production (8–10) and β -cell failure (11), developing fasting hyperglycemia at 6–8 wks of age and severe type 2 diabetes at 10–12 wks of age (8). IRS2 also coordinates IGF-1/IGF1R signaling in the central nervous system, where this factor is essential for the regulation of cell proliferation, growth, differentiation and metabolic demands during fetal and postnatal development (12).

Address correspondence to Silvia Murillo-Cuesta, Institute of Biomedical Research Alberto Sols (CSIC-UAM), Arturo Duperler 4, 28029 Madrid, Spain. Phone: +34-91-5854421; Fax: +34-91-5854401; E-mail: smurillo@iib.uam.es.

Submitted September 5, 2011; Accepted for publication November 29, 2011; Epub (www.molmed.org) ahead of print December 1, 2011.

Human *IGF1* mutations cause severe neural defects including microcephaly, mental retardation and profound deafness (13–16). Similarly, *Igf1*^{-/-} mice exhibit delayed myelination (17,18), severe sensorineural deafness (19,20) and progressive blindness (21). The cochlea of IGF-1-deficient mice presents an abnormal tectorial membrane, increased neuronal apoptosis, poor myelination of nerve fibers (22,23) and impaired activation of protein kinase B (PKB; AKT) and rapid accelerated fibrosarcoma (RAF) kinases (24).

Irs2^{-/-} mice also show impaired brain growth (25), defects in myelination (26) and increased apoptosis in the retina (27). Therefore, there is a close relationship between insulin and IGF-1 functions and signaling pathways in the central nervous system, reflected in the similar neural phenotypes of both *Irs2*^{-/-} and *Igf1*^{-/-} mice. However, the specific role of IRS2 in the inner ear of the IRS2-deficient mice remains unstudied.

Recently, it has been shown that the diabetic phenotype in IRS2-deficient mice can be reverted by the inhibition of the protein tyrosine phosphatase (PTP)-1B (28,29). PTP1B directly interacts with both IR and IGF1R and catalyzes the dephosphorylation of both tyrosine kinase receptors (30,31). The importance of PTP1B as a modulator of insulin action has been shown both *in vivo* in liver and muscle (32–34), as well as in cellular models. Mice lacking the *Ptpn1* gene exhibit increased insulin sensitivity, resistance to weight gain on a high-fat diet and increased basal metabolic rate (35,36). The role of PTP1B in IGF-1-mediated signaling in nervous and sensorial systems remains less studied. Accordingly, we have analyzed the hearing function and cochlear morphology of *Irs2*^{-/-} mice and the impact of PTP1B deficiency.

MATERIALS AND METHODS

Mouse Housing and Handling

Three genetically modified mouse strains (*Irs2*^{-/-}*Ptpn1*^{+/+}, *Irs2*^{+/+}*Ptpn1*^{-/-} and *Irs2*^{-/-}*Ptpn1*^{-/-}) maintained in a mixed

C57BL/6 × 129/Sv genetic background (28) were used in the study. Because the impact of the *Irs2* gene mutation on the metabolic phenotype is variable (8,37), the detailed study of hearing was carried out only in male mice that developed type 2-like diabetes, defined as glycemia >300 mg/dL. Glucose concentration was measured in tail-vein blood samples using a blood glucose meter (Accu-Check Aviva; Roche Diagnostics, Sant Cugat del Vallés, Spain). Type 2-like diabetes in IRS2-deficient mice normally starts at ~8 wks, with a high mortality rate at ~16 wks of age as a result of diabetic complications (37). Considering this time course, functional and morphological assessment was performed in prediabetic (young 3–5 wks old) and diabetic (adult 8–16 wks old) mice. Fed glucose levels were 123.8 ± 2.6, 198 ± 15.7, 118.6 ± 3.19 and 127.6 ± 3.5 mg per 100 mL in *Irs2*^{+/+}*Ptpn1*^{+/+}, *Irs2*^{-/-}*Ptpn1*^{+/+}, *Irs2*^{+/+}*Ptpn1*^{-/-} and *Irs2*^{-/-}*Ptpn1*^{-/-} 5-wk-old mice, respectively. Fed glucose levels were maintained in the normal range in 12-wk-old mice of the *Irs2*^{+/+}*Ptpn1*^{+/+} (138.8 ± 2.6), *Irs2*^{+/+}*Ptpn1*^{-/-} (132.7 ± 3) and *Irs2*^{-/-}*Ptpn1*^{-/-} (129.6 ± 3.5) genotypes, but were dramatically increased to 426.8 ± 35.7 mg/100 mL in the *Irs2*^{-/-}*Ptpn1*^{+/+} mice.

Mice were fed ad libitum with a standard diet and drinking water and controlled following Federation of European Laboratory Animal Science Associations (FELASA) recommendations. All animal experimentation was conducted in accord with Spanish and European legislation and approved by the Spanish National Research Council (CSIC) Animal Care and Use Committee.

Hearing Evaluation

Hearing was evaluated by studying the auditory brainstem response (ABR) following standard methods (19,20). Click and 8- to 40-kHz tone burst stimuli were generated with SigGenRP™ software (Tucker-Davis Technologies, Alachua, FL, USA) and presented from 90 to 20 decibel sound pressure level (dB SPL) in 5–10 dB SPL steps. The electrical

response was amplified, recorded and averaged, and hearing thresholds were determined for each stimulus as described (19). Peak and interpeak latencies were analyzed at 90 dB SPL after click stimulation. *Irs2*^{+/+}*Ptpn1*^{+/+} mice of matched ages were used as controls.

ABR data were analyzed using SPSS v19.0 software. For each age group, ABR parameters were compared among genotypes with analysis of variance and Bonferroni and Tamhane *post hoc* multiple comparisons. The results were considered significant at $P \leq 0.05$. Data in the text are expressed as mean ± standard deviation (SD).

Cochlear Morphology and Stereology

Mouse cochleae were processed as reported (20,22). Cochleae were embedded in paraffin wax (Panreac Quimica, Castellar del Valles, Spain) or methacrylate (Technovit 7100; Heraeus-Kulzer, Wehrheim, Germany). Sections of 5 or 40 μm thickness were stained with hematoxylin-eosin or 0.1% cresyl violet (Fluka; Sigma-Aldrich Quimica, Tres Cantos, Spain), respectively. Cochlear morphology was studied with an Axio-phot Zeiss microscope plus Olympus DP70 digital camera. Immunohistochemical studies were performed on paraffin sections to detect myelin P0 (Neuromics; 1:100), neurofilament 200 kDa (Diagnostic; 1:100), potassium channel Kir4.1 (Chemicon; 1:400) and myosin VIIa (Proteus Biosciences; 1:100), combined with the appropriate biotin-conjugated secondary antibody solution (Chemicon; dilution 1:200). A tertiary antibody solution (ExtrAvidin® peroxidase, combined with 3,3-diaminobenzidine tetrahydrochloride [DAB] or Texas Red® Streptavidin; Vector Laboratories; 1:200) was used to detect biotin. Sections were mounted in Entellan® (Merck Chemicals, Mollet del Vallés, Spain) for light microscopy or in Vectashield® (Vector Laboratories) for confocal microscopy analysis (Leica TCS SP2). Quantification of myelin P0 immunoreactivity was performed on photomicrographs taken with 24 bits of red-green-blue (RGB)

color depth using a 12-bit DP70 digital camera in an Olympus BX51 microscope. All pictures were taken with a 20× UPlanSApo Olympus objective, using the same settings. Densitometry of the immunoreactivity was performed with National Institutes of Health (NIH) Image J software. Optical density measures were obtained on freehand-delineated profiles covering all the cell bodies present in four to five immunoreacted sections per case. Four cases per group were studied.

The method of Cavalieri (38,39) was used to estimate the total volume of main cochlear structures, by point counting on target regions identified in systematically sampled sections throughout the cochlea. The interactive test grids and control of the motorized stage were provided by the CAST stereological software package (v.2,3,2,0; Visiopharm). Live images were captured with an Olympus DP70 solid-state video camera and projected on a high-resolution video monitor at a magnification of 300×. Every third section of the cochlea was studied, which enabled 5–11 sections of each target structure to be sampled and measured. The precision of the estimates was determined by the coefficient of error (CE) as described for systematic random samples (37). The different average CEs obtained with this sampling scheme ranged between 3% and 7%. Volume estimates were not corrected for shrinkage.

Cochlear Protein Extraction and Western Blot Analysis

Frozen cochleae from 5-wk-old mice were pooled (three mice per genotype) and lysed in 200 μ L ice-cold radioimmunoprecipitation assay buffer containing 0.01% of protease and phosphatase inhibitor cocktails (P8340, P5726; Sigma Aldrich) and cochlear extracts prepared as reported (24). Protein concentration was determined by Micro BCA Protein Assay Kit (PIERCE Biotechnology-Thermo Fisher Scientific) using bovine serum albumin (BSA) as the standard. Analysis of protein expression was performed by Western blotting. Cochlear

proteins were subjected to sodium dodecyl sulfate–polyacrylamide gel electrophoresis and transferred to polyvinylidene fluoride membranes in a Bio-Rad Trans Blot apparatus. After incubation with a blocking solution, the membranes were probed overnight at 4°C with primary antibodies for phospho-p38 MAPK (Cell Signaling Technologies; 1:1,000), phospho-p44/42 MAPK (Cell Signaling Technologies; 1:5,000), PTP-1B (Millipore; 1:5,000), p-Akt1/2/3 (Ser 473)-R (Santa Cruz Biotechnology; 1:1,000) and p38 α (Santa Cruz Biotechnology; 1:5,000) as a loading control. Antibodies were diluted in Tris-buffered saline with Tween containing 5% BSA for phosphorylation-specific antibodies or nonfat dried milk for others. The membranes were washed and incubated with the corresponding peroxidase-conjugated secondary antibodies for 1 h at room temperature. Immunoreactive bands were visualized by enhanced chemiluminescence (GE Healthcare) using X-ray films (Agfa), and the bands were quantified by densitometry with NIH Image J software. Different exposure times were used to ensure that bands were not saturated. Statistical significance was estimated by Student *t* test. *P* values of <0.05 were considered significant.

RESULTS

IRS2 Deficiency Results in Congenital Sensorineural Deafness in Mice

Irs2^{+/+}*Ptpn1*^{+/+} (hereafter referred as wild-type) mice analyzed at 3–5 wks of age showed normal hearing thresholds and ABR wave patterns, whereas *Irs2*^{-/-}*Ptpn1*^{+/+} mice presented a profound sensorineural deafness with no ABR response to stimuli below 70 dB SPL. These differences in hearing phenotype were maintained in the adult 8- to 16-wk-old mice group (Figure 1A). *Irs2*^{-/-}*Ptpn1*^{+/+} mice showed significantly (*P* ≤ 0.001) elevated hearing thresholds in response to click stimulus at both 3–5 wks (80 ± 10 dB SPL, *n* = 7) and 8–16 wks (79 ± 8, *n* = 18), compared with wild-type

mice of matched ages (39 ± 3 dB SPL, *n* = 9, and 36 ± 4, *n* = 8, respectively) (Figure 1B and Table 1). Accordingly, both 3- to 5-wk-old and 8- to 16-wk-old deaf *Irs2*^{-/-}*Ptpn1*^{+/+} mice presented a significant (*P* ≤ 0.001) hearing loss at all frequencies studied, but with high frequencies (28 and 40 kHz) being most affected, whereas control wild-type mice presented normal hearing thresholds at all frequencies studied (Figure 1C). Differences in ABR thresholds for pure tones between *Irs2*^{-/-}*Ptpn1*^{+/+} mice and wild-type counterparts were of 30–40 dB SPL (Table 1).

Peak latencies of *Irs2*^{-/-}*Ptpn1*^{+/+} mice were significantly increased, thus suggesting a delay in the transmission of the stimulus from the cochlea to the inferior colliculus in the brainstem. Concretely, peak I latency in *Irs2*^{-/-}*Ptpn1*^{+/+} mice was significantly greater (*P* ≤ 0.001, *n* = 6) than in wild-type mice. In addition, statistically significant differences were found in interpeak latencies II–IV and I–IV. Therefore, the delay in transmission originates in the cochlea and is maintained along the auditory pathway (Table 1 and Figure 1D). The increase in ABR thresholds and peak I latency observed in the young *Irs2*^{-/-}*Ptpn1*^{+/+} mice and sustained through time suggest that the deficiency of IRS2 is associated with congenital neurosensorial deafness that could not be compensated during cochlear postnatal maturation.

The amplitude/intensity and latency/intensity curves for peak I in both young and adult *Irs2*^{-/-}*Ptpn1*^{+/+} mice were also altered. Peak I amplitudes were lower than those from wild-type mice, whereas the curve for peak I latency was situated above that of wild-type mice (data not shown).

PTP1B Deficiency Does Not Affect Hearing and Improves Hearing Function in IRS2-Deficient Mice

To study the effect of the absence of PTP1B in the hearing function of IRS2-deficient mice, *Irs2*^{+/+}*Ptpn1*^{-/-} and *Irs2*^{-/-}*Ptpn1*^{-/-} mice were studied. *Irs2*^{+/+}*Ptpn1*^{-/-} mice did not exhibit any

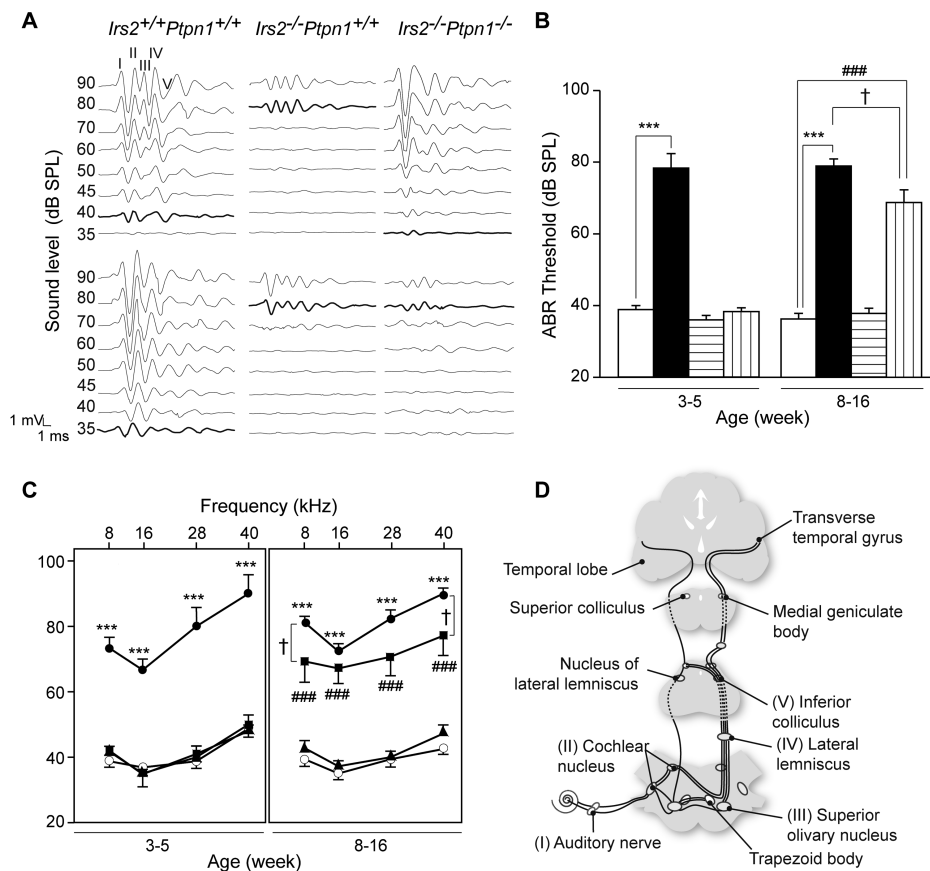


Figure 1. Hearing function. (A) Representative ABR recordings in response to click stimuli of wild-type, *Irs2^{-/-}Ptpn1^{+/+}* and *Irs2^{-/-}Ptpn1^{-/-}* mice at 5 (upper row) and 11 (bottom row) wks of age. *Irs2*-deficient mice showed profound deafness compared with the normal ABR pattern of the wild-type mice, at both ages studied. Double-null mice developed severe hearing loss during the time window studied. (B) ABR thresholds (mean \pm standard error of the mean (SEM)) in response to click stimuli in wild-type (□), *Irs2^{-/-}Ptpn1^{+/+}* (■), *Irs2^{+/+}Ptpn1^{-/-}* (▤) and *Irs2^{-/-}Ptpn1^{-/-}* (▨) mice, at both ages studied. Wild-type and *Irs2^{+/+}Ptpn1^{-/-}* mice maintained normal hearing thresholds during the study. Statistically significant differences were found between *Irs2*-deficient mice and normal hearing genotypes at both ages ($***P < 0.001$), whereas double-null mice presented significantly raised thresholds only in adulthood ($###P < 0.001$). (C) ABR thresholds in response to tone burst stimuli (8–40 kHz) in wild-type (○), *Irs2^{-/-}Ptpn1^{+/+}* (●), *Irs2^{+/+}Ptpn1^{-/-}* (▲) and *Irs2^{-/-}Ptpn1^{-/-}* (■) at both ages studied. *Irs2*-null mice showed an all-frequency involved hearing loss, with statistically significant differences compared with wild-type ($***P < 0.001$) and *Irs2^{+/+}Ptpn1^{-/-}* mice, which maintained normal thresholds throughout the study. The lack of PTP1B in *Irs2^{-/-}Ptpn1^{-/-}* mice delayed and tempered the increase of the audiogram with statistically significant differences, with control mice appearing only in the adult age ($###P < 0.001$). Thresholds for 4 and 40 kHz were significantly lower in double-null mice compared with *Irs2^{-/-}Ptpn1^{+/+}* mice ($†P < 0.05$). (D) Scheme of the auditory pathway, indicating the main structures and the correspondence with ABR peaks. Cochlear ganglion neurons connect with the cochlear nuclei, which project into the lateral lemniscus via acoustic striae and afterwards in the nucleus of the inferior colliculus. Neurons in the inferior colliculus project to the medial geniculate body of the thalamus that sends tonotopical projections to the primary auditory cortex. Several accessory auditory brain stem nuclei send both crossed and uncrossed projections through the lateral lemniscus.

obvious alteration in the ABR parameters and presented mean click threshold values similar to, and frequently even better than those of wild-type mice (3- to 5-wk-old mice: 36 ± 4 dB SPL, $n = 10$; 8- to 16-wk-old mice: 38 ± 4 , $n = 9$; Figures 1A, B; Table 1). In addition, the audiogram of both young and adult *Irs2^{+/+}Ptpn1^{-/-}* mice was similar to that of wild-type mice, with ABR thresholds in response to tone bursts ~ 40 dB SPL for all the frequencies analyzed (Figure 1C; Table 1). No significant differences were found in peak I latency compared with wild-type mice (Table 1). Both amplitude-intensity and latency-intensity curves in *Irs2^{+/+}Ptpn1^{-/-}* mice were similar to those of wild-type mice at the two ages analyzed (not shown).

Interestingly, whereas young *Irs2^{-/-}Ptpn1^{-/-}* mice did not show hearing loss, the adult population presented signs of deafness. Accordingly, *Irs2^{-/-}Ptpn1^{-/-}* mice at 8–16 wks of age displayed moderate deafness with ABR click thresholds of 69 ± 10 dB SPL ($n = 8$), which showed significant differences when compared with wild-type mice ($P \leq 0.001$, $n = 8$) and *Irs2^{+/+}Ptpn1^{-/-}* mice ($P \leq 0.001$, $n = 9$), and even when compared with severely deaf *Irs2^{-/-}Ptpn1^{+/+}* mice ($P < 0.05$, $n = 18$) (Figure 1B, Table 1). Adult *Irs2^{-/-}Ptpn1^{-/-}* mice also showed an impaired response to pure tone bursts, especially at high frequencies (Figure 1C, Table 1) and elevated interpeak latencies (Table 1) associated with aging. In addition, amplitude-intensity and latency-intensity curves in adult *Irs2^{-/-}Ptpn1^{-/-}* mice were close to those of *Irs2^{+/+}Ptpn1^{+/+}* mice (not shown). Therefore, the concomitant absence of PTP1B delayed the onset of the deafness.

IRS2-Deficient Mice Present Alterations in the Stria Vascularis and Cochlear Ganglion

General cochlear morphology of wild-type, *Irs2^{-/-}Ptpn1^{+/+}* and *Irs2^{-/-}Ptpn1^{-/-}* mice were similar at both ages, and the main cochlear structures in the scala media showed an apparent normal cytoarchitecture (Figures 2A–I). Accordingly,

Table 1. ABR thresholds and latencies.

n	Genotype							
	Age 3–5 wks				Age 8–16 wks			
	<i>Irs2^{+/+}Ptpn1^{+/+}</i>	<i>Irs2^{-/-}Ptpn1^{+/+}</i>	<i>Ptpn1^{-/-}Irs2^{+/+}</i>	<i>Irs2^{-/-}Ptpn1^{-/-}</i>	<i>Irs2^{+/+}Ptpn1^{+/+}</i>	<i>Irs2^{-/-}Ptpn1^{+/+}</i>	<i>Ptpn1^{-/-}Irs2^{+/+}</i>	<i>Irs2^{-/-}Ptpn1^{-/-}</i>
n	9	7	10	6	8	18	9	8
ABR threshold (dB SPL)								
Click	39 ± 3	80 ± 10 ^a	36 ± 4	38 ± 3	36 ± 4	79 ± 8 ^a	38 ± 4	69 ± 10 ^a
8 kHz	39 ± 5	73 ± 6 ^a	42 ± 4	42 ± 4	39 ± 6	81 ± 8 ^a	43 ± 5	69 ± 17 ^a
16 kHz	37 ± 7	67 ± 6 ^a	35 ± 12	35 ± 3	35 ± 5	72 ± 10 ^a	37 ± 5	67 ± 12 ^a
20 kHz	39 ± 7	80 ± 10 ^a	41 ± 8	40 ± 8	39 ± 7	82 ± 11 ^a	40 ± 6	71 ± 15 ^a
40 kHz	49 ± 4	90 ± 10 ^a	48 ± 6	50 ± 7	43 ± 5	90 ± 7 ^a	47 ± 8	77 ± 16 ^a
n	9	6	9	6	8	18	9	8
Peak latency (ms)								
I	1.28 ± 0.08	1.39 ± 0.14 ^a	1.35 ± 0.0	1.32 ± 0.06	1.28 ± 0.09	1.32 ± 0.08 ^c	1.30 ± 0.10	1.26 ± 0.09
II	2.16 ± 0.09	2.30 ± 0.13 ^b	2.36 ± 0.07 ^c	2.28 ± 0.05	2.20 ± 0.12	2.17 ± 0.12	2.12 ± 0.10 ^c	2.16 ± 0.04
IV	3.88 ± 0.12	4.14 ± 0.90 ^a	4.48 ± 0.20	4.22 ± 0.09 ^a	3.85 ± 0.15	3.93 ± 0.14	3.83 ± 0.14	3.96 ± 0.15
Interpeak latency (ms)								
I–II	0.87 ± 0.10	0.90 ± 0.05	1.01 ± 0.07 ^c	0.95 ± 0.04 ^b	0.92 ± 0.10	0.84 ± 0.09 ^c	0.82 ± 0.11 ^c	0.90 ± 0.08
II–IV	1.72 ± 0.13	1.84 ± 0.09 ^c	2.12 ± 0.16	1.94 ± 0.06 ^a	1.65 ± 0.14	1.76 ± 0.09 ^c	1.71 ± 0.08	1.79 ± 0.11 ^c
I–IV	2.59 ± 0.09	2.75 ± 0.12 ^c	3.13 ± 0.21	2.89 ± 0.06 ^a	2.57 ± 0.10	2.60 ± 0.13	2.53 ± 0.15	2.69 ± 0.15

ABR thresholds (mean ± SD in dB SPL) in response to click and tone burst (4–40 kHz) stimuli were determined in young (3- to 5-wk-old) and adult (8- to 16-wk-old) mice from the four genotypes analyzed. Click ABR peak and interpeak latencies (mean ± SD, in ms) are shown in the four genotypes studied at the two ages analyzed. Statistically significant differences were found when comparing mutant mice with wild-type mice:

^a*P* < 0.001.

^b*P* < 0.05.

^c*P* < 0.01.

the sensory hair cells in the organ of Corti appeared normal (Figures 2J, L, N), and the pattern of expression of myosin VIIa, a specific marker for the inner and outer hair cells, was similar in the mutant and wild-type mice (Figures 2K, M, O).

The stria vascularis is a three-layer structure, formed by marginal, intermediate and basal cells and highly vascularized by intraepithelial capillaries, which produces the endolymph and maintains the endocochlear potential (Figure 2C). In wild-type mice, the stria vascularis showed a normal histological organization and capillary network (Figures 3A, C), with the marginal cells displaying extensive folds surrounding the endostrial capillaries (Figures 3B, D), as well as a normal pattern of expression of the potassium channel Kir4.1 (40) (Figures 3E, F). In contrast, the *Irs2^{-/-}Ptpn1^{+/+}* mice showed traits of stria atrophy at both ages (Figure 3G–J, brackets), including

marginal cell degeneration (Figures 3G–J, arrows), dilatation or merging of the capillaries (Figures 3G, H; dashed arrows) and altered Kir4.1 expression (Figures 3K, L). Accordingly, stereological evaluation of stria volume showed a significant decrease in *Irs2^{-/-}Ptpn1^{+/+}* mice when compared with wild-type mice (Figure 4, stria vascularis [StV]). In the *Irs2^{-/-}Ptpn1^{-/-}* mice, the stria vascularis did not show gross volume changes, although signs of degeneration were evident (Figures 3M–P), showing a large number of merged capillaries, specially at 11 wks of age (Figures 3O, P; dashed arrows) and altered Kir4.1 expression (Figures 3Q, R).

Histological analysis of the cochlear ganglia showed a similar cellular organization among genotypes (Figures 5A–C). However, since alterations in the myelination of IRS2-deficient mice have been reported (26), myelin P0 was used to detect

possible defects in this process. Indeed, 11-wk-old *Irs2^{-/-}Ptpn1^{+/+}* and *Irs2^{-/-}Ptpn1^{-/-}* mice showed alterations in the myelin P0 expression pattern compared with wild-type mice (Figures 5D–F). Quantification of myelin P0 immunoreactivity in the cochlear ganglion indicated a statistically significant reduction in *Irs2^{-/-}Ptpn1^{+/+}* (43.9%, *P* < 0.05) and *Irs2^{-/-}Ptpn1^{-/-}* (33.8%, *P* < 0.05) mice regarding wild-type mice values. Accordingly, both myelin P0 and neurofilament 200-kDa immunostaining of fibers projecting from the cochlear ganglion to the sensory cells were also altered in IRS2-deficient mice (Figures 5H, I, K, L; arrows) compared with wild-type mice (Figures 5G, J), thus suggesting deficits in the density of innervation of the hair cells, in concordance with the reduction in the cochlear ganglion volume (Figure 4; SG).

In contrast to IRS2-deficient mice and accordingly with the functional data,

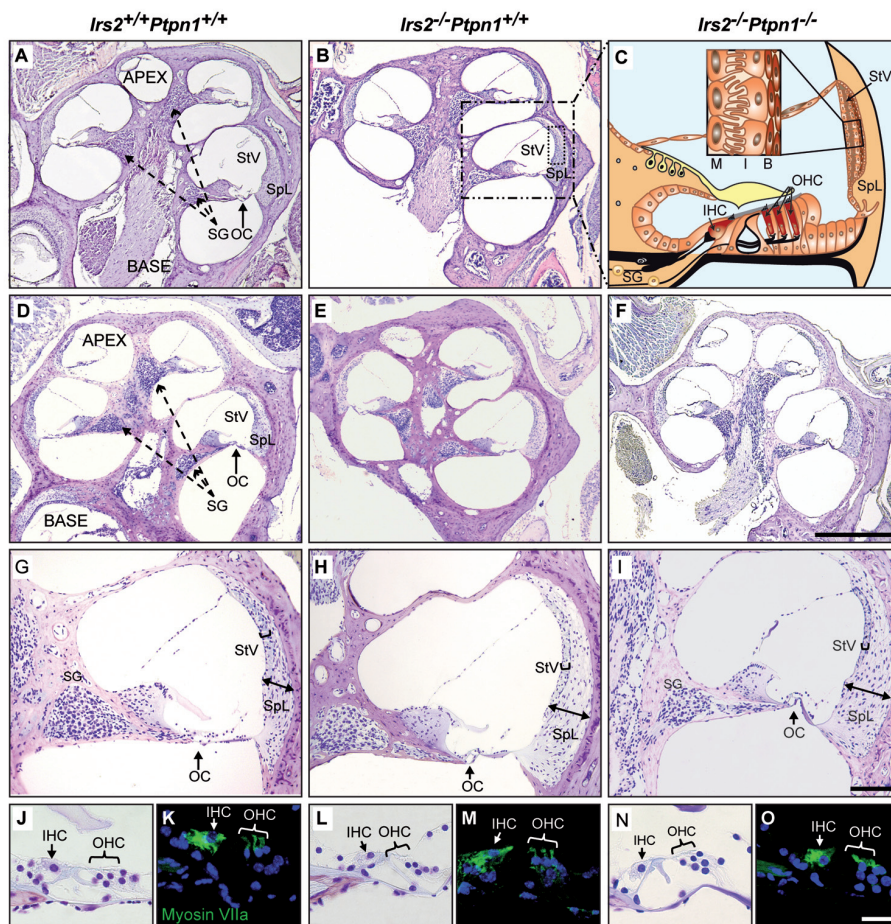


Figure 2. General cochlear morphology. (A–F) Hematoxylin-eosin staining of midmodiolar paraffin sections of the cochlea at postnatal wk 5 (A, B) and 11 (D–F) in *Irs2*^{+/+}*Ptpn1*^{+/+}, *Irs2*^{-/-}*Ptpn1*^{+/+} and *Irs2*^{-/-}*Ptpn1*^{-/-} mice. The general cochlear histology of both *Irs2*^{-/-}*Ptpn1*^{+/+} and *Irs2*^{-/-}*Ptpn1*^{-/-} mutants (B, E, F) was similar to that in the wild-type mice (A, D), with no obvious alterations, at either age studied. (C) Drawing scheme of the cochlear duct of the basal turn (highlighted in B) and detail of the stria vascularis (StV, small rectangle), which is formed by the basal (B), the intermediate (I) and the marginal (M) cell layers and contains a dense capillary network. (G–I) Hematoxylin-eosin staining of the cochlear duct of the basal turn in *Irs2*^{+/+}*Ptpn1*^{+/+} (G), *Irs2*^{-/-}*Ptpn1*^{+/+} (H) and *Irs2*^{-/-}*Ptpn1*^{-/-} mice (I) at postnatal wk 11. Both mutants showed a developed organ of Corti (OC), cochlear ganglion (SG), stria vascularis (StV) and spiral ligament (SpL). The bracket and double head arrow indicate the thickness of the stria vascularis and the spiral ligament, respectively. (J, L, N) Higher magnification of the organ of Corti in *Irs2*^{+/+}*Ptpn1*^{+/+}, *Irs2*^{-/-}*Ptpn1*^{+/+} and *Irs2*^{-/-}*Ptpn1*^{-/-} mice at postnatal wk 11 illustrating that the outer hair cells (OHC) and inner hair cells (IHC), as well as the surrounding supporting cells, were normal in appearance in both mutants (L, N) compared with the control wild-type mice (J). (K, M, O) Myosin VIIa expression in the inner hair cells (IHC) and outer hair cells (OHC) was unaffected in both mutants (M, O). Scale bars: A, B, D–F, 500 μ m; G–I, 100 μ m; J–O 25 μ m.

general cochlear morphology in *Irs2*^{+/+}*Ptpn1*^{-/-} mice was similar to that of control mice (Figures 6A, B), and the main cochlear structures, including cochlear ganglion and stria vascularis

presented normal features (Figures 6C–H), with the later showing a normal pattern of expression of the potassium channel Kir4.1 compared with control mice (Figures 6I, J).

Analysis of the IGF-1 Signaling Pathways in IRS2-Deficient Mice

The levels of PTP1B, p-AKT, p-p38 and p-p44/42 MAPKs were measured by Western blotting in 5-wk-old mice cochleae. MAPKs play an important role in inner ear development. Alterations in the phosphorylation levels of MAPKs and AKT in the deaf *Igf1*-null mouse have been described (24,41). PTP1B protein was expressed in the cochlea of the wild-type and *Irs2*^{-/-}*Ptpn1*^{+/+} mice. PTP1B was slightly increased in IRS2-deficient mice (Figure 7) as reported previously (28). As expected, PTP1B expression was totally lost in the *Irs2*^{+/+}*Ptpn1*^{-/-} (Figure 7) and *Irs2*^{-/-}*Ptpn1*^{-/-} mice (not shown). IGF-1 signaling pathways were studied, and a statistically significant reduction in the levels of p-MAPK was observed in the 5-wk-old double mutant mice, as reported for the *Igf1*^{-/-} mouse (24). In contrast, the phosphorylation levels of AKT and p38 α did not show differences.

DISCUSSION

IRS2 coordinates IGF-1/IGF1R signaling in the nervous system, and accordingly, its deletion in mice leads to reduced neural proliferation during development (25), defects in appropriate timing of myelination (26) and loss of retinal photoreceptors by increased apoptosis (27). Given the similar neural phenotype of both *Igf1*- and *Irs2*-null mice, we hypothesized that lack of IRS2 could also lead to hearing impairment in the same way as it happens in *Igf1*^{-/-} mice (14,19). Here we have investigated for the first time the hearing function and cochlear morphology of *Irs2*^{-/-}*Ptpn1*^{+/+} mice and the effects of genetic ablation of PTP1B.

The hearing phenotype in *Irs2*^{-/-}*Ptpn1*^{+/+} mice included increased ABR thresholds, particularly for high frequencies, and a delay in peak I latency that spreads along the auditory pathway. These features are similar to those observed in the *Igf1*^{-/-} mice (19,20) and also in patients carrying homozygous *IGF1* mutations (15,16). Therefore, understanding

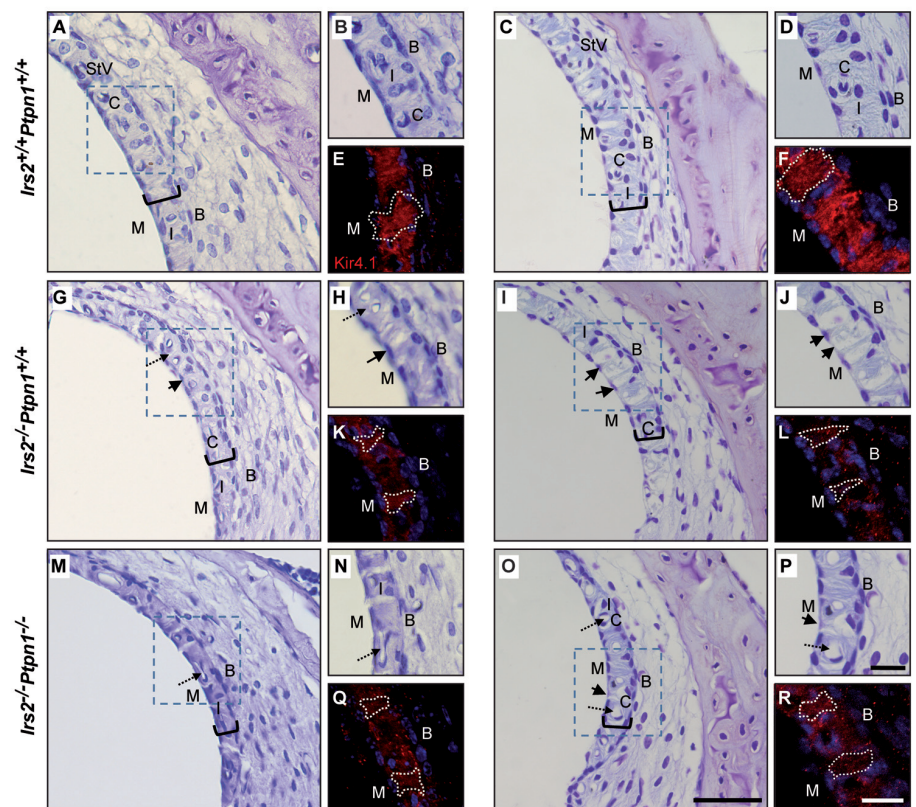


Figure 3. Morphology of the stria vascularis. Hematoxylin-eosin staining of the stria vascularis at the cochlear basal turn in *Irs2*^{+/+}*Ptpn1*^{+/+} (A–D), *Irs2*^{-/-}*Ptpn1*^{+/+} (G–J) and *Irs2*^{-/-}*Ptpn1*^{-/-} mice (M–P) at 5 wks (left column) and 11 wks (right column) of age is shown. Wild-type mice showed normal morphology, vasculature pattern and thickness (bracket) of the stria vascularis (A–D). (B, D) Amplified detail of the stria vascularis illustrating the three epithelial layers, the basal, the intermediate and the marginal cell layers and the normal capillary network. *Irs2*^{-/-}*Ptpn1*^{+/+} mice present numerous intercellular spaces, probably because of degeneration of the marginal cells (arrows) and the merging of the capillaries (dashed arrows) (G–J). At postnatal wk 5, *Irs2*^{-/-}*Ptpn1*^{-/-} mice show a slight atrophy of the stria vascularis with few intercellular spaces (dashed arrows) (M and N). The degeneration process worsens with age and 11-wk-old double-null mice show severe atrophy and a number of merged capillaries (dashed arrows) (O, P). (E, F, K, L, Q, R) Laser confocal microscopic examination showing Kir4.1 immunoreactivity (red). In control mice, immunostaining appeared as a fold-like structure at the basolateral side of marginal cells, designating the normal invaginations of these cells (dotted white line in E and F). Both mutant mice show a significant reduction in Kir4.1 expression and an irregular shape of the invaginations of the marginal cells (dotted white line in K, L, Q and R). B, basal cells; C, capillary network; I, intermediate cells; M, marginal cell; StV, stria vascularis. Scale bars: A, C, G, I, M, O: 50 μ m; B, D, H, J, N, P: 25 μ m; E, F, K, L, Q, R: 25 μ m.

the role of IRS2 in hearing function is crucial to identify new sites for therapeutic intervention on hearing loss. Interestingly, *Irs2*^{-/-}*Ptpn1*^{+/+} mice with obvious hearing impairment at young ages usually developed a diabetic phenotype with fasting hyperglycemia (>300 mg/dL) at 8–16 wks of life, and ABR data were

used as a predictive tool for type 2 diabetes diagnosis in mice. Many clinical and epidemiological studies have shown a direct relationship between type 2 diabetes and hearing loss, especially in the elderly, with a pattern similar to presbycusis (42). Histopathological findings in patients

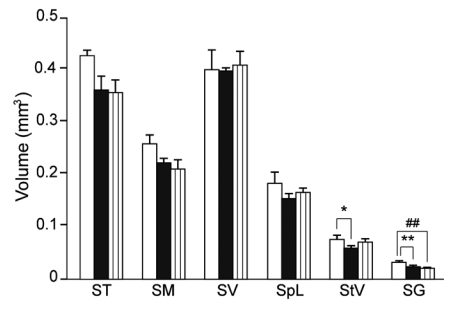


Figure 4. Cochlear volumes. Volume (mean \pm SEM, mm³) of the tympanic (ST), media (SM) and vestibular (SV) scalas and the spiral ligament (SpL), stria vascularis (StV) and cochlear ganglion (SG) in wild-type (n = 3), *Irs2*^{+/+}*Ptpn1*^{+/+} (n = 4), and *Irs2*^{-/-}*Ptpn1*^{-/-} (n = 4) mice at 11 wks of age is shown. The smaller size of ST, SM and SpL in *IRS2*-deficient and double-null mice compared with wild-type mice did not reach significance. However, SG was significantly reduced in size in both *IRS2*-deficient (**P* < 0.05) and double-null mice (***P* < 0.01) compared with wild-type mice; StV also showed a decrease in volume, but only in *IRS2*-deficient mice (**P* < 0.05; ***P* < 0.01). □, *Irs2*^{+/+}*Ptpn1*^{+/+} mice; ■, *Irs2*^{-/-}*Ptpn1*^{+/+} mice; ▨, *Irs2*^{-/-}*Ptpn1*^{-/-} mice.

with type 2 diabetes include cochlear microangiopathy, degeneration of the stria vascularis and outer hair cells (43). Diabetes might affect the vasculature and neural system of the inner ear, leading to hearing impairment that was manifested in around 50% of the diabetic patients studied (44,45). In addition, genetic, pharmacological and nutritional animal models were used to study the effects of type 2 diabetes on hearing (46,47). Vasilyeva *et al.* (47) reported elevation of ABR thresholds as early as 2 months after induction of type 2 diabetes in CBA/CaJ mice. Similarly, ob/ob C57BL/6J mice showed significant differences in ABR thresholds during aging compared with control mice and histological findings that include outer hair cell degeneration and loss of cochlear ganglion cells in the middle and basal cochlear turns (46). In contrast to these models of type 2 diabetes, the *Irs2*-null mice studied herein

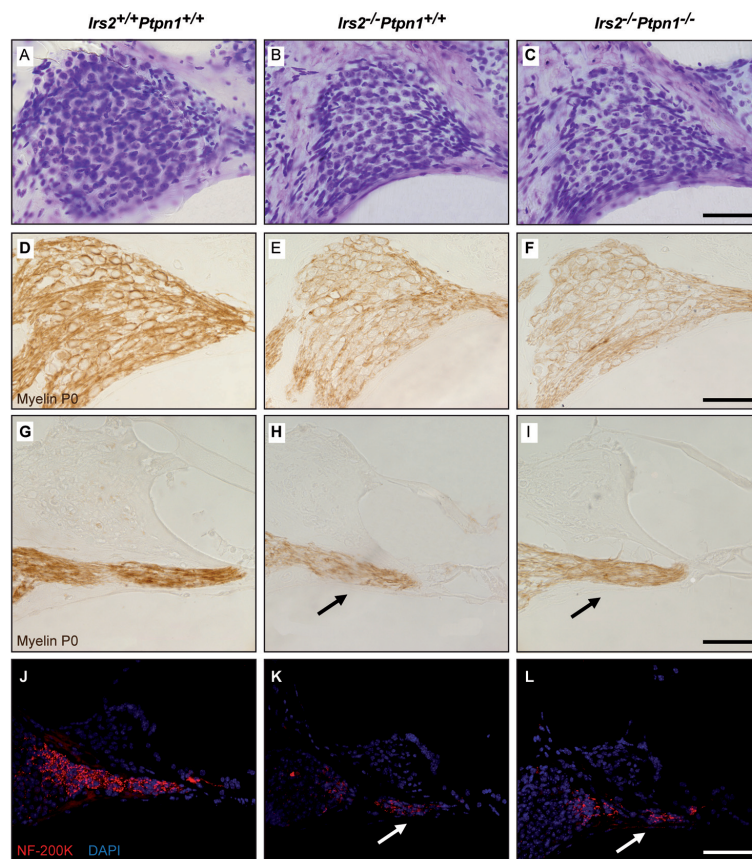


Figure 5. Cochlear ganglion and nerve fibers. (A–C) Cresyl violet staining of midmodiolar methacrylate sections of the cochlear ganglion at the cochlear basal turn in *Irs2*^{+/+}*Ptpn1*^{+/+} (A), *Irs2*^{-/-}*Ptpn1*^{+/+} (B) and *Irs2*^{-/-}*Ptpn1*^{-/-} mice (C) at postnatal wk 11. A slight reduction in the cellular density was more evident in both mutants (B, C) compared with wild-type (A). (D–F) Myelin P0 immunostaining of the cochlear ganglion shows less intense labeling in *Irs2*^{-/-}*Ptpn1*^{+/+} (E) and *Irs2*^{-/-}*Ptpn1*^{-/-} (F) mice than in control mice (D). (G–I) Accordingly, myelin P0 immunostaining of nerve fibers projecting from the cochlear ganglion to the sensory cells is less intense in *Irs2*^{-/-}*Ptpn1*^{+/+} and *Irs2*^{-/-}*Ptpn1*^{-/-} (arrows in H and I) than in wild-type mice (G). (J–L) Similarly, a weaker neurofilament 200-kDa immunostaining is observed in *Irs2*^{+/+}*Ptpn1*^{-/-} (K, white arrow) and *Irs2*^{-/-}*Ptpn1*^{-/-} (L, white arrow) mice compared with wild-type mice (J). Scale bars: A–I, 50 μ m; J–L, 75 μ m.

showed hearing impairment at one month of age before developing hyperglycemia, indicating that hearing loss is not only a direct consequence of chronically raised glucose levels. These data suggest that hearing evaluation may have a prognostic value for the clinical follow-up of diabetic patients.

In addition to the hearing impairment, we have found that IRS2 deficit is associated with a reduced myelin P0 and neurofilament staining in the cochlear ganglia. This hypoinnervation could be due

to a reduction in the number of nerve fibers and/or in the myelin content. IGF-1 is required for the late differentiation of the cochlear ganglion neurons and thus for the correct innervation of the cochlea (24). Accordingly, the cochlear ganglion of *Igf1*-null mice presents a significant decrease in the number and size of neurons and hypomyelination (20,22). These data suggest that IGF-1 actions on the innervation of the cochlear ganglia could be mediated by signaling through IRS2.

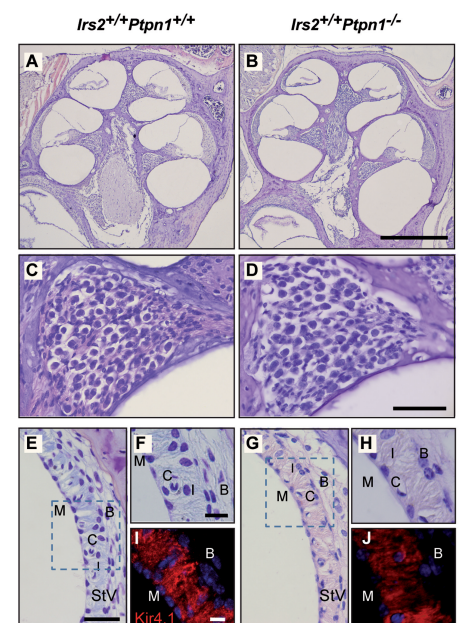


Figure 6. Cochlear morphology of the *Irs2*^{+/+}*Ptpn1*^{-/-} mice. (A–D) Hematoxylin-eosin staining of midmodiolar paraffin sections of the cochlea (A, B) and cochlear ganglion (C, D) in wild-type and *Irs2*^{+/+}*Ptpn1*^{-/-} mice at postnatal wk 11. No gross differences were found. (E–H) Hematoxylin-eosin staining of the stria vascularis at the cochlear basal turn in wild-type (E, F) and *Irs2*^{+/+}*Ptpn1*^{-/-} (G, H) mice showed normal morphology, vasculature pattern and thickness in both genotypes. Details of the stria vascularis (F, H) illustrating the basal, intermediate and marginal cell layers and the normal capillary network are shown. (I, J) Kir4.1 immunoreactivity (red) revealed no evident differences between genotypes. Scale bars: A, B, 500 μ m; C, D, E, G, 50 μ m; F, H, I, J, 25 μ m. B, basal cells; C, capillary network; I, intermediate cells; M, marginal cell.

IRS2-deficient mice also showed a degeneration of the stria vascularis, similar but earlier than that observed in aged 12-month-old *Igf1*^{-/-} mice (20). Degeneration of the stria vascularis is a common feature in presbycusis and in other pathologies that deal with sensorineural hearing loss such as systemic hypertension, certain autoimmune diseases and diabetes mellitus (43,48). Histopathological findings in diabetic

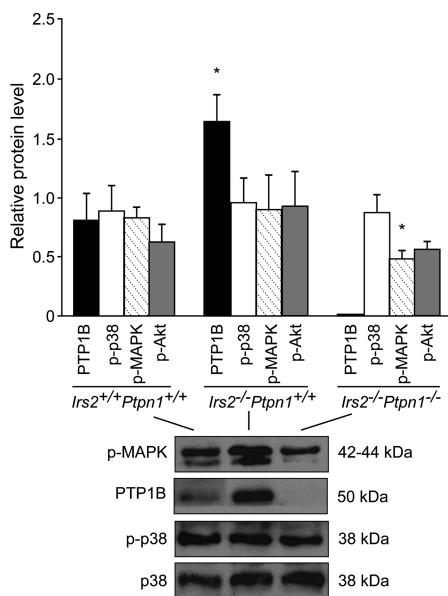


Figure 7. PTP1B, p-p38, p-MAPK and p-Akt protein levels. PTP1B, p-p38, p-MAPK and p-Akt levels were measured by Western blotting in 5-wk-old mice cochleae. P38 α was used as a loading control to calculate the relative protein levels. Values are presented as mean \pm SEM of at least three mice per condition. Statistical significance was estimated by *t* test; *P* values of <0.05 were considered significant. PTP1B expression levels were significantly increased in *Irs2*^{-/-}*Ptpn1*^{+/+} mice compared with wild-type mice ($*P < 0.05$), and p-MAPK levels decreased when comparing the double mutant with the wild-type mice ($*P < 0.05$).

patients and animal models of diabetes include alterations in the structure of the marginal cells, widening of the strial intercellular spaces and microvascular disease (43,48) and are usually attributed to sustained raised glucose levels. These changes are similar to that observed in IRS2-deficient mice, even without hyperglycemia. Delayed strial degeneration in *Irs2*^{-/-}*Ptpn1*^{-/-} compared with *Irs2*^{-/-}*Ptpn1*^{+/+} mice might be due to better metabolic control in the double mutant, as it happens in the liver (28).

In addition, *Irs2*^{-/-}*Ptpn1*^{+/+} and *Irs2*^{-/-}*Ptpn1*^{-/-} mice presented an altered pattern of Kir4.1 immunoreactiv-

ity in the marginal cells when compared with wild-type mice. Deletion or changes in the expression of this channel, even without extensive degeneration of the stria vascularis, compromise the maintenance of the endocochlear potential that allows sensory transduction (49,50).

PTP1B deficiency did not show any obvious hearing phenotype at the ages studied, but partially compensated the prediabetic sensorineural hearing loss caused by the lack of IRS2. Indeed, young *Irs2*^{-/-}*Ptpn1*^{-/-} mice showed normal hearing function, but developed neurosensorial deafness with increased ABR thresholds at 8–16 wks of life. The expression levels of PTP1B and its association with the IR are increased in the liver of hyperglycemic *Irs2*^{-/-}*Ptpn1*^{+/+} mice, resulting in a blockade of compensatory IR/IRS1-mediated insulin signaling (28). Therefore, PTP1B deficiency normalizes fasting blood glucose, fed blood glucose, peripheral insulin sensitivity and glucose tolerance in *Irs2*^{-/-}*Ptpn1*^{-/-} mice at 12–16 wks of age, compared with highly insulin-resistant and glucose-intolerant *Irs2*^{-/-}*Ptpn1*^{+/+} mice of the same age (28,34). In contrast, the deaf phenotype observed in *Irs2*^{-/-}*Ptpn1*^{+/+} mice cannot be completely reverted by deletion of the *Ptpn1* gene, which only delays the onset of hearing loss in double-null mutant mice. These results suggest that there are additional players downstream of IRS2 signaling involved in the development of hearing, with this key issue deserving further investigation.

Our results show for the first time that PTP1B is expressed in the cochlea and that its expression is upregulated by an IRS2 deficit, as reported in the liver (28). Increased PTP1B expression and activity cause dephosphorylation of target receptors and blockade of downstream signaling. Thus, PTP1B upregulation has been proposed as the molecular mechanism underlying the loss of sensitivity to insulin in the liver of hyperglycemic *Irs2*^{-/-} mice. Accordingly, lack of PTP1B in the double mu-

tant favors enhanced compensatory intracellular response to insulin that in the liver is mediated by IRS1 (28). Here we report that damage of cochlear function in the IRS2 mutant is delayed when PTP1B is absent, suggesting that a similar mechanism is operating in the cochlea.

CONCLUSION

In summary, the results presented in this study demonstrate for the first time a unique tissue-specific role of IRS2 in cochlear development and hearing function; therefore, the *Irs2*^{-/-} mouse could be a novel model for the *in vivo* study of hearing loss associated with altered glucose metabolism. Our data also suggest that modulation of PTP1B activity could be a pharmacological target of interest for the sensory syndromes associated with diabetes.

ACKNOWLEDGMENTS

We thank Julie Chowen (Hospital Niño Jesús, Madrid) for the critical reading of the manuscript and comments and J Pérez, R Martínez-Vega (Institute of Biomedical Research), D Morales, A De Las Heras (Medical School, Autonoma University of Madrid) and J Contreras (Veterinary Faculty, Complutense University of Madrid) for technical and scientific support. This work was supported by the Ministerio de Ciencia e Innovacion (SAF2008-00470 and SAF2011 to I Varela-Nieto and SAF2009-08114 to AM Valverde) and the Fundacion Mutua Madrileña to IV Varela-Nieto. S Murillo-Cuesta, A González-Rodríguez and G Camarero hold postdoctoral contracts from the CIBERER, CIBERDEM and CSIC Junta para la Ampliación de Estudios (JAE) programs, respectively.

DISCLOSURE

The authors declare that they have no competing interests as defined by *Molecular Medicine*, or other interests that might be perceived to influence the results and discussion reported in this paper.

REFERENCES

- White MF. (2006) Regulating insulin signaling and beta-cell function through IRS proteins. *Can. J. Physiol. Pharmacol.* 84:725–37.
- Taniguchi CM, Emanuelli B, Kahn CR. (2006) Critical nodes in signalling pathways: insights into insulin action. *Nat. Rev. Mol. Cell. Biol.* 7:85–96.
- Thirone AC, Huang C, Klip A. (2006) Tissue-specific roles of IRS proteins in insulin signaling and glucose transport. *Trends Endocrinol. Metab.* 17:72–8.
- White MF. (2002) IRS proteins and the common path to diabetes. *Am. J. Physiol. Endocrinol. Metab.* 283:E413–22.
- Accili D, et al. (1996) Early neonatal death in mice homozygous for a null allele of the insulin receptor gene. *Nat. Genet.* 12:106–9.
- Liu JP, et al. (1993) Mice carrying null mutations of the genes encoding insulin-like growth factor I (Igf-1) and type 1 IGF receptor (Igf1r). *Cell.* 75:59–72.
- Araki E, et al. (1994) Alternative pathway of insulin signalling in mice with targeted disruption of the IRS-1 gene. *Nature.* 372:186–90.
- Withers DJ, et al. (1998) Disruption of IRS-2 causes type 2 diabetes in mice. *Nature.* 391:900–4.
- Kubota N, et al. (2000) Disruption of insulin receptor substrate 2 causes type 2 diabetes because of liver insulin resistance and lack of compensatory beta-cell hyperplasia. *Diabetes.* 49:1880–9.
- Previs SF, et al. (2000) Contrasting effects of IRS-1 versus IRS-2 gene disruption on carbohydrate and lipid metabolism in vivo. *J. Biol. Chem.* 275:38990–4.
- Withers DJ, et al. (1999) Irs-2 coordinates Igf-1 receptor-mediated beta-cell development and peripheral insulin signalling. *Nat. Genet.* 23:32–40.
- LeRoith D. (2008) Insulin-like growth factors and the brain. *Endocrinology.* 149:5951.
- Bonapace G, Concolino D, Formicola S, Strisciuglio P. (2003) A novel mutation in a patient with insulin-like growth factor 1 (IGF1) deficiency. *J. Med. Genet.* 40:913–7.
- Murillo-Cuesta S, et al. (2011) The role of insulin-like growth factor-I in the physiopathology of hearing. *Front Mol. Neurosci.* 4:11.
- Walenkamp MJ, et al. (2005) Homozygous and heterozygous expression of a novel insulin-like growth factor-I mutation. *J. Clin. Endocrinol. Metab.* 90:2855–64.
- Woods KA, Camacho-Hubner C, Savage MO, Clark AJ. (1996) Intrauterine growth retardation and postnatal growth failure associated with deletion of the insulin-like growth factor I gene. *N. Engl. J. Med.* 335:1363–7.
- D'Ercole AJ, Ye P, O'Kusky JR. (2002) Mutant mouse models of insulin-like growth factor actions in the central nervous system. *Neuropeptides.* 36:209–20.
- Zeger M, et al. (2007) Insulin-like growth factor type 1 receptor signaling in the cells of oligodendrocyte lineage is required for normal in vivo oligodendrocyte development and myelination. *Glia.* 55:400–11.
- Cediel R, et al. (2006) Sensorineural hearing loss in insulin-like growth factor I-null mice: a new model of human deafness. *Eur. J. Neurosci.* 23:587–90.
- Riquelme R, et al. (2010) A comparative study of age-related hearing loss in wild type and insulin-like growth factor I deficient mice. *Front Neuroanat.* 4:27.
- Rodriguez-de la Rosa L, et al. (2012) Age-related functional and structural retinal modifications in the Igf1(-/-) null mouse. *Neurobiol. Dis.* 2012, Feb 28 [Epub ahead of print].
- Camarero G, et al. (2001) Delayed inner ear maturation and neuronal loss in postnatal Igf-1-deficient mice. *J. Neurosci.* 21:7630–41.
- Sanchez-Calderon H, Milo M, Leon Y, Varela-Nieto I. (2007) A network of growth and transcription factors controls neuronal differentiation and survival in the developing ear. *Int. J. Dev. Biol.* 51:557–70.
- Sanchez-Calderon H, et al. (2010) RNA microarray analysis in prenatal mouse cochlea reveals novel IGF-I target genes: implication of MEF2 and FOXM1 transcription factors. *PLoS One.* 5:e8699.
- Schubert M, et al. (2003) Insulin receptor substrate-2 deficiency impairs brain growth and promotes tau phosphorylation. *J. Neurosci.* 23:7084–92.
- Freude S, et al. (2008) IRS-2 branch of IGF-1 receptor signaling is essential for appropriate timing of myelination. *J. Neurochem.* 107:907–17.
- Yi X, et al. (2005) Insulin receptor substrate 2 is essential for maturation and survival of photoreceptor cells. *J. Neurosci.* 25:1240–8.
- Gonzalez-Rodriguez A, et al. (2010) Inhibition of PTP1B restores IRS1-mediated hepatic insulin signaling in IRS2-deficient mice. *Diabetes.* 59:588–99.
- Kushner JA, et al. (2004) Islet-sparing effects of protein tyrosine phosphatase-1b deficiency delays onset of diabetes in IRS2 knockout mice. *Diabetes.* 53:61–6.
- Buckley DA, et al. (2002) Regulation of insulin-like growth factor type I (IGF-I) receptor kinase activity by protein tyrosine phosphatase 1B (PTP-1B) and enhanced IGF-I-mediated suppression of apoptosis and motility in PTP-1B-deficient fibroblasts. *Mol. Cell. Biol.* 22:1998–2010.
- Seely BL, et al. (1996) Protein tyrosine phosphatase 1B interacts with the activated insulin receptor. *Diabetes.* 45:1379–85.
- Clampit JE, et al. (2003) Reduction of protein-tyrosine phosphatase-1B increases insulin signaling in FAO hepatoma cells. *Biochem. Biophys. Res. Commun.* 300:261–7.
- Egawa K, et al. (2001) Protein-tyrosine phosphatase-1B negatively regulates insulin signaling in I6 myocytes and FaO hepatoma cells. *J. Biol. Chem.* 276:10207–11.
- Gum RJ, et al. (2003) Reduction of protein tyrosine phosphatase 1B increases insulin-dependent signaling in ob/ob mice. *Diabetes.* 52:21–8.
- Elchebly M, et al. (1999) Increased insulin sensitivity and obesity resistance in mice lacking the protein tyrosine phosphatase-1B gene. *Science.* 283:1544–8.
- Klaman LD, et al. (2000) Increased energy expenditure, decreased adiposity, and tissue-specific insulin sensitivity in protein-tyrosine phosphatase 1B-deficient mice. *Mol. Cell. Biol.* 20:5479–89.
- Garcia-Barrado MJ, et al. (2011) Differential sensitivity to adrenergic stimulation underlies the sexual dimorphism in the development of diabetes caused by Irs-2 deficiency. *Biochem. Pharmacol.* 81:279–88.
- Garcia-Finana M, Cruz-Orive LM. (2000) New approximations for the variance in cavalieri sampling. *J. Microsc.* 199:224–38.
- Gundersen HJ, et al. (1988) Some new, simple and efficient stereological methods and their use in pathological research and diagnosis. *APMIS.* 96:379–94.
- Hibino H, et al. (1997) An ATP-dependent inwardly rectifying potassium channel, KAB-2 (Kir4.1), in cochlear stria vascularis of inner ear: its specific subcellular localization and correlation with the formation of endocochlear potential. *J. Neurosci.* 17:4711–21.
- Magarinos M, et al. (2010) RAF kinase activity regulates neuroepithelial cell proliferation and neuronal progenitor cell differentiation during early inner ear development. *PLoS One.* 5:e14435.
- Kakarlapudi V, Sawyer R, Staecker H. (2003) The effect of diabetes on sensorineural hearing loss. *Otol. Neurotol.* 24:382–6.
- Fukushima H, et al. (2006) Effects of type 2 diabetes mellitus on cochlear structure in humans. *Arch. Otolaryngol. Head Neck Surg.* 132:934–8.
- Austin DF, et al. (2009) Diabetes-related changes in hearing. *Laryngoscope.* 119:1788–96.
- Bainbridge KE, Hoffman HJ, Cowie CC. (2008) Diabetes and hearing impairment in the United States: audiometric evidence from the National Health and Nutrition Examination Survey, 1999 to 2004. *Ann. Intern. Med.* 149:1–10.
- Lee HS, et al. (2008) Early sensorineural hearing loss in ob/ob mouse, an animal model of type 2 diabetes. *Clin. Exp. Otorhinolaryngol.* 1:211–16.
- Vasilyeva ON, et al. (2009) Interactions of hearing loss and diabetes mellitus in the middle age CBA/CaJ mouse model of presbycusis. *Hear. Res.* 249:44–53.
- Frisina ST, et al. (2006) Characterization of hearing loss in aged type II diabetics. *Hear. Res.* 211:103–13.
- Hibino H, Kurachi Y. (2006) Molecular and physiological bases of the K⁺ circulation in the mammalian inner ear. *Physiology (Bethesda).* 21:336–45.
- Rozenfurt N, et al. (2003) Time course of inner ear degeneration and deafness in mice lacking the Kir4.1 potassium channel subunit. *Hear. Res.* 177:71–80.